Consistent use of the Gurson-Tvergaard damage model for the R-curve calculation

Gabriele Cricrì
University of Salerno, Department of Mechanical Engineering; gcricri@unisa.it

ABSTRACT. The scope of the present work is to point out a consistent simulation procedure for the quasi-static fracture processes, starting from the micro-structural characteristics of the material. To this aim, a nine-parameters Gurson-Tvergaard damage law has been used. The damage parameters depend on the micro-structural characteristics and have to be calculated, measured or opportunely tuned. This can be done, as proposed by the author, by using an opportunely tuned GT model for the representative volume element simulations, in order to enrich the original damage model by considering also the defect size distribution. Once determined all the material parameters, an MT fracture test has been simulated by a FEM code, to calculate the R-curve in an aeronautical Al-based alloy. The simulation procedure produced results in a very good agreement with the experimental data.

KEYWORDS. Ductile fracture; Damage tolerance; Microvoids.

INTRODUCTION

In aircraft structures the damage tolerance design concept is widely used, that tolerates the presence of macroscopic cracks during the ordinary service life, prescribing to take they under control. The fuselage skin, which thickness ranges from 1 to 3 mm, is often made of aeronautical aluminium alloys capable of fully ductile behaviour. For this reason, a great importance assumes in this field the study of both the static and the dynamic response of cracked panels in ductile regime, in terms of residual strength. The so-called R-curve, that gives the critical stress intensity factor versus the crack length for a given panel, is a widely used tool to design following the above criteria; unfortunately it depends both from material and geometrical properties and then changes as the test configuration changes. A reliable calculation model of the R-curve is, for this reasons, very important for the design purposes, in order to drastically decrease the amount of physical tests.
Many models for ductile fracture growth have been proposed in the past [1-7] and, for their relative simplicity and efficiency the Gurson-Tvergaard model and many its variants are proposed by several authors and also included in some public FEM codes. They typically present many free parameters that should be calibrated [8-10] and fixed in a consistent way in order to make the calculation procedure effective. In the present work, a complete procedure to calculate the R-curve is presented and an application on a widely used aeronautical alloy is reported, using some material and test data provided by industrial research offices.

THE GURSON MODEL FOR DUCTILE FRACTURE

In an homogeneous metal model, the total deformation usually doesn't affect the volume change, because the plastic part of the deformation is dominant with respect to the elastic one. Otherwise, in a microstructure model containing voids, volume can *globally* change, due to the local plastic flow arising around the voids boundary. Consequently, the

microstructure response to an imposed global strain will be a stress curve with a softening, nevertheless the material matrix be constituted by a metal with an hardening behaviour. Contemporarily, the voids grow until the global load carry capability becomes negligible.
This model is able to explain the local strength decrease during the fracture process of ductile metals in the intermediate phase between the *nucleation* and the *coalescence* of voids. In other words, in the void growth model the number of voids is kept constant. Nucleation and coalescence are taken into account before the homogenization, applying some opportune corrections directly to the stress-strain cell response.

Gurson-Tvergaard model

The homogenization technique is based on the stress-strain characterization of a Representative Volume Element (RVE), that is the minimum material volume containing all the micro-structural information of an heterogeneous material, related to the specific problem under investigation (see, e.g., [11, 12]). In the Gurson-Tvergaard void growth model, the RVE of the material is considered as a *cubic* volume with a single void, existing before the material is stressed. The initial void volume fraction f_0 should be chosen as the 'equivalent' volume fraction corresponding to the physical distribution of voids or defects inside the RVE (Fig.1).

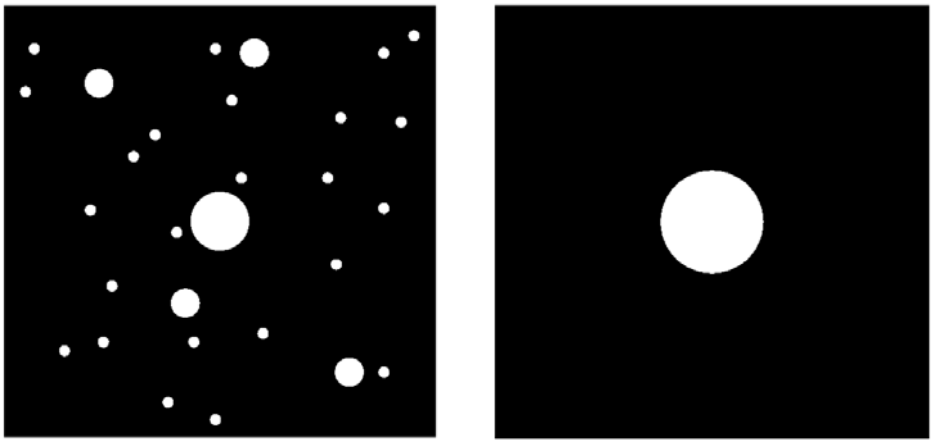

Figure 1: Physical vs. equivalent voids distribution

The resulting homogenized material model was defined by modifying the analytical solution of the second cell in fig. 1, performed by Gurson and limited to a rigid-plastic material model of the matrix. The corrections take into account for the hardening of the matrix material and for the presence of void cell array instead of a single void cell. They are represented by the coefficients q_1, q_2, q_3 in the critical surface definition, introduced by Tvergaard.
The homogenized constitutive law is defined by (tensor are indicated with bold characters):

$$\phi\left(\sigma_{eq},\sigma_m,\bar{\sigma},f\right)=\left(\frac{\sigma_{eq}}{\bar{\sigma}}\right)^2+2q_1 f\cosh\left(\frac{3q_2\sigma_m}{2\bar{\sigma}}\right)-\left(1+q_3 f\right)^2=0 \tag{1$_1$}$$

$$d\boldsymbol{\varepsilon}^p=d\lambda\frac{\partial\phi}{\partial\boldsymbol{\sigma}} \tag{1$_2$}$$

$$df=\left(1-f\right)d\boldsymbol{\varepsilon}^p:\boldsymbol{I} \tag{1$_3$}$$

$$\left(1-f\right)\bar{\sigma}d\bar{\varepsilon}=\boldsymbol{\sigma}:d\boldsymbol{\varepsilon}^p \tag{1$_4$}$$

$$\boldsymbol{\sigma}=\boldsymbol{D}\left(\boldsymbol{\varepsilon}-\boldsymbol{\varepsilon}^p\right) \tag{1$_5$}$$

$$d\bar{\varepsilon}=\begin{cases}\dfrac{N\varepsilon_0}{\sigma_0}\left(\dfrac{\bar{\sigma}}{\sigma_0}\right)^{N-1}d\bar{\sigma} & \text{if } \phi=0 \text{ and } d\bar{\sigma}>0\\ 0 & \text{otherwise}\end{cases} \tag{1$_6$}$$

Where:

(1_1) defines the critical surface;
(1_2) is the plastic flow rule;
(1_3) is the void growth rate definition;
(1_4) imposes the equivalence between micro and macro-mechanical plastic work;
(1_5) is the global stress-strain relationship;
(1_6) is the plastic hardening power law for the matrix material.

Further:

$\boldsymbol{\sigma}$	: stress tensor;
$\boldsymbol{\varepsilon}, \boldsymbol{\varepsilon}^p$	: total and plastic strain tensors;
σ_{eq}	: Von Mises equivalent global stress;
σ_m	: global mean stress;
$\bar{\sigma}$	: current matrix flow stress (internal variable);
$\bar{\varepsilon}$	: current matrix equivalent strain (internal variable);
f	: voids volume fraction (internal variable);
N	: hardening coefficient;
σ_0, ε_0	: yield equivalent stress and strain;
q_1, q_2, q_3	: Tvergaard correction coefficients.

Nucleation model

The nucleation of the first void in an array of cells is implicit in the above model. With the increasing load, other voids can nucleate in the RVE, and this fact is taken into account in the homogenized material law by increasing the void growth rate defined in (1_3).

In the present study the following relation is used:

$$df_{nuc} = A(\bar{\varepsilon})\, d\bar{\varepsilon} \qquad (2_1)$$

where:

$$A(\bar{\varepsilon}) = \frac{f_N}{S_N\sqrt{2\pi}} \exp\left[-\frac{1}{2}\left(\frac{\bar{\varepsilon}-\varepsilon_N}{S_N}\right)^2\right] \qquad (2_2)$$

The corrected void growth rate becomes:

$$df = (1-f)\, d\boldsymbol{\varepsilon}^p : \boldsymbol{I} + A(\bar{\varepsilon})\, d\bar{\varepsilon} \qquad (1'_3)$$

The expressions (2) relate the voids growth rate due to the nucleation process to the internal equivalent strain rate $d\bar{\varepsilon}$. This acceleration is driven by the parameter A and it is limited to an internal strain condition in which $\bar{\varepsilon}$ is quite close to a certain value ε_N, representing the matrix strain value in which the nucleation takes place.

Three new parameter are so introduced in the constitutive law (1):

f_N	: magnitude of the volume fraction rate increasing;
ε_N	: main value in which the nucleation takes place
S_N	: standard deviation.

Cell dimension

It is well known that the undefined equilibrium problem in a material domain which constitutive law has softening branches loses ellipticity near the critical point, so it is hill-posed.
If the finite element method is used to search a solution, disregarding the above problem, the resulting discrete equation can be solved, but the solution is chronically mesh dependent and the convergence can't be reached. This occurs because near the softening condition the strain field becomes discontinuous and, correspondently, in the discretized problem the strain tends to concentrate in a small zone, which size depends on the elements size. Smaller the element size, smaller the zone affected by the strain concentration. This behaviour is commonly named *localization*.
If the softening law derives from a physical model of the material, the incongruence can be explained noting that, at the micro-structural scale, the material domain can't be longer be considered homogeneous, so the softening at the large scale material law can be attributed to the micro-structural *geometric* changes.
Apparently, the consequence of this fact is that we can't use homogenization techniques if the global material law presents a softening behaviour. In practice, using a FEM model, we can avoid the mesh dependence by keeping fix the element dimensions in the fracture zone, regardless with the macroscopic geometry of the domain. The correct element dimension depends on the scale of the local fracture process related to the particular material under consideration. In this way, the element dimension becomes a further parameter of the material constitutive law.
In other words, we couldn't use an homogenized law because the analytical equilibrium problem is hill-posed, but the error that can't be eliminated in the FEM solution of this problem can be *driven* in order to reach an allowable numerical result.

Voids coalescence

In the constitutive law (1) the internal strain state is represented by an *unique* variable $\overline{\varepsilon}$. This simplification can be accepted in the early phases of the void growth, in which the internal strain (and stress) distribution doesn't vary too much. In the following load phase the material model becomes unrealistic. This is the phase in which the fracture advances between two consecutive voids (coalescence) an even the RVE model with the single equivalent void becomes unrealistic.
The coalescence, and the consequent crack advancing, is modelled in the FEM code by the elimination of the corresponding element (killed element) when a critical volume fraction value f_c is reached. Many studies have demonstrate that the critical value should be much less then 1, that is the value provided by the theory. For many material the critical volume fraction can be set-up between 0.15 ÷ 0.25, and a phenomenological correlation furnish the following empirical law:

$$f_c = 0.15 + 2 f_0 \tag{3}$$

Along the crack plane, the element traction forces are still present in this condition ($f = f_c$) and they are gradually decreased until zero is reached, using a multiplicative coefficient γ, related to the cell dimension D and depending from a further parameter λ, to be set.

$$\gamma = 1.0 - \frac{\overline{D} - \overline{D}_0}{\lambda D} \qquad (0 \le \gamma \le 1.0) \tag{4}$$

CELL CALIBRATION

The material model descript above needs the calculation, the measurement or the phenomenological tuning of (at least) *13* parameters:

The internal plastic-hardening parameters N, σ_0, ε_0 .
The Tvergaard correction coefficients q_1, q_2, q_3 .
The nucleation parameters f_N , ε_N , S_N .
The cell height D.
The initial and critical void volume fraction f_0 , f_c .

The force release parameter λ.

Critical void volume fraction and force release parameter

These parameters are related to the coalescence phase. For the present calibration they have been chosen as mean values from the ones present in literature.

f_c = 0.2; λ = 0.1.

The release forces parameter contributes to form the energy released in the element extinction process, so it can't be considered a merely calculation parameter. The γ coefficient (4) depends on the orthogonal to the crack plane component of the strain. In fact, we can write:

$$\gamma = 1.0 - \frac{\overline{D} - \overline{D}_0}{\lambda D} \cong 1.0 - \frac{\overline{D}/D - \overline{D}_0/D}{\lambda} = 1 - \frac{\exp(\varepsilon) - \exp(\varepsilon_c)}{\lambda}$$

$$\sigma_{release} = \gamma \sigma_c$$

So, the energy W released in the force release process (coalescence) can be evaluated:

$$W = ADw = \int_{\varepsilon_c}^{\varepsilon(\gamma=0)} \gamma \sigma_c d\varepsilon \cong \sigma_c AD \frac{\lambda}{2} = V \sigma_c \frac{\lambda}{2} \quad \text{(for small } \lambda, \varepsilon_c\text{)}$$

where:

σ_c is the stress corresponding to the critical strain ε_c (reached when $f = f_c$);
D, A are the cell height and the cell area parallel to the crack plane;
V is the cell volume.

Cell height and initial void volume fraction

Both the cell height and the initial void volume fraction can be estimated considering as a starting point the defect size distribution.

2024A-T351 All Three Directions							
Equivalent Diameter (μm)	Volume Fraction (%)	Standard Deviation	Nearest Neighbour (μm)	Nearest Neighbour Standard Deviation(μm)	Minimum Separation Distance (μm)	Minimum Separation Distance Standard Deviation (μm)	Average Diam of particles in size category (μm)
All Sizes	0,76	0,33	10,61	8,01	8,55	8,09	1,75
1:2	0,13	0,06	16,14	12,11	14,65	12,39	1,41
2:3	0,10	0,05	35,18	26,48	32,82	27,30	2,41
3:4	0,07	0,04	62,38	46,78	59,61	48,71	3,41
4:6	0,12	0,07	58,90	40,68	53,76	42,22	4,87
6:8	0,11	0,08	93,54	64,45	86,12	66,44	6,88
8:10	0,09	0,09	130,27	96,68	122,14	101,91	8,86
10+	0,14	0,21	126,95	97,90	111,94	99,72	13,23

Table 1: Defects size (industrial data)

The cell dimension, and in particular the cell height, is a fundamental parameter because, when the strain localization occurs, the cell height coincides with the localized strip of material. So, from this point, the most of the energy released is proportional to the this parameter. On the other side, in the present model the energy released is also influenced by the coalescence parameters and by the shape of the stress-strain curve (that depends on the nucleation and Tvergaard

parameters). Then, the correct cell height should be chosen taking into account the influence of the above parameters in the fracture process.
If we consider the cell as a representative volume element (as it should be) it should contain a sufficiently representative defect (considered as voids) distribution.
Of course, a greater RVE contains more micro-structural information, but is less useful in the present model because the strain would localize in a strip with *fixed* height. In conclusion, the cell height can't be precisely defined without a critical consideration of all the constitutive law parameters influence.
As an approximate evaluation, we can consider the bigger defects above the last 20% of the total volume fraction the driving defects of the localization process. In this way, with reference to the Tab.1, an RVE, which dimension is coincident with the cell height, will contain *one* defect with 10+ μm diameter and the appropriate number of minor defects as deduced from the size distribution (Tab. 2).

Category	Volume fraction	Average diameter (μm)	Spherical average diameter (μm)	Volume (μm^3)	Density (defects/ mm^3)	Defects in the RVE
1:2	0,0013	1,41	1,79	3,00	433000	904
2:3	0,0010	2,41	3,07	15,1	66200	138
3:4	0,0007	3,41	4,34	42,8	16300	34
4:6	0,0012	4,87	6,20	125	8810	18
6:8	0,0011	6,88	8,50	322	3410	7
8:10	0,0009	8,86	11,3	752	1200	2
10+	0,0014	13,23	17,7	2920	479	1

Table 2: Defects distribution in the RVE (from Tab. 1 data rearranging).

The cell height and the initial void volume fraction can be finally estimated:

$$D = (\text{10+ category density})^{-1/3} \approx 130\ \mu m; \quad f_0 = 0.0014$$

The D value is in good agreement with the literature values that varies between 80÷200 μm.
This procedure can appear arbitrary. In fact, if the categories was chosen in a different way (for instance the last category could be 8+ or 12+), the resulting D and f_0 parameters were different. On the other side, this can be avoided if we consider for all the distribution, as stated above, the bigger defects above the last 20% of the total volume fraction; in this case, is arbitrary the 20% value.
As discussed above, a certain arbitrariness is un-eliminable because the cell height (and consequently the initial volume fraction) has the double role of dimension of the RVE and dimension of the strain localization zone. Then, once established the cell height on the basis of a reasonable RVE choice, the effect of the strain localization should be taken into account by tuning both the nucleation parameters (that can be considered responsible for the minor defects growth) and the coalescence parameters f_c , λ.
As an example, in the pictures below (Fig. 2) is reported the equivalent strain distribution inside two different bidimensional RVE with the same initial volume fraction (see Fig.1 for the undeformed configuration). The first, is the simplified Gurson RVE with a single void; the second, has a void distribution compatible with the Tab. 2 distribution.
It can be deduced that the localization zone dimension is larger in the first that in the second RVE. This fact influences the global cell response (Fig. 3). Supposing that the second RVE represents a sufficiently accurate evaluation of the material behaviour, the cell height is too large in relation to the 'true' localization zone, as it results comparing the different entity of energy involved in the load process. Once established a compromise value D = 100 μm < 130 μm, the difference should be taken into account by tuning, as written above, the nucleation and the coalescence parameters.

Tvergaard correction coefficients

The correction coefficients q_1, q_2, q_3 can be calculated from a single void RVE model.
The global cell behaviour has been calculated for two different load conditions:

1) Imposed global strain $\varepsilon_x > 0$ and free surface condition for y and z direction.
2) Imposed global strain $\varepsilon_x > 0$ and $\varepsilon_y = \varepsilon_z = -0.2\ \varepsilon_x$.

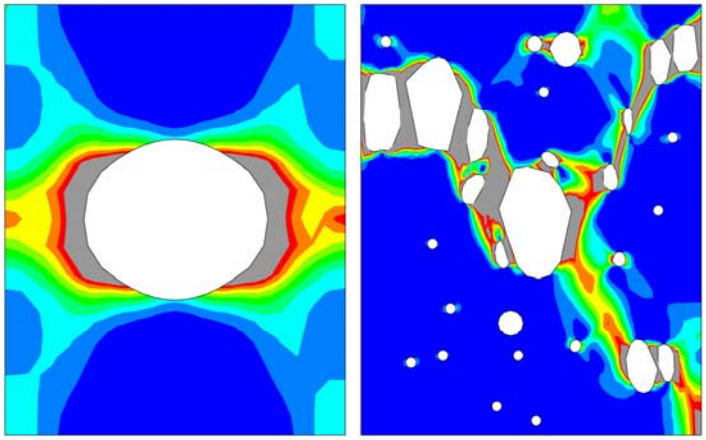

Figure 2: Equivalent strain distribution inside two RVE

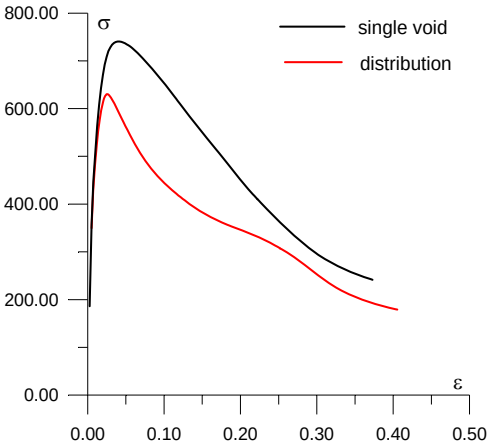

Figure 3: Global cell response.

In the following pictures 4-5 are presented the cell mesh and the resulting strain distribution in the x direction for the two considered load cases.

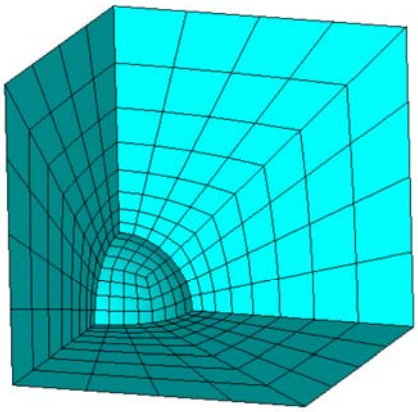

Figure 4: FEM model of the single void cell

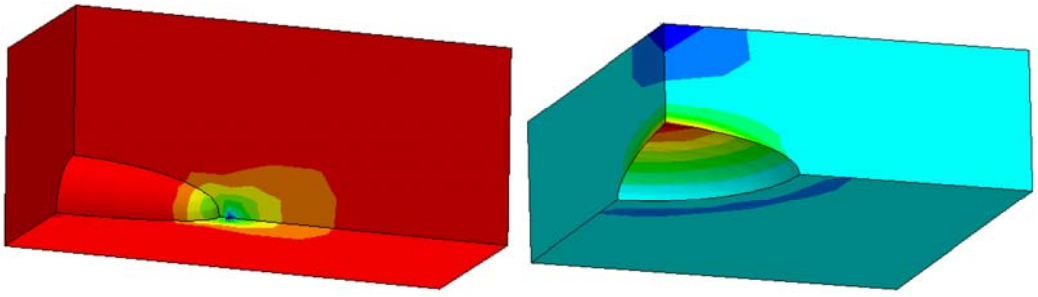

Figure 5: Strain (ε_x) distribution for the two load cases

It can be noted that in the first case the x-direction strain is about uniform, but in the second there is a consistent strain concentration on the void boundary. This agrees with the constitutive law (1), that attributes the void volume fraction growth to the mean stress (eq. 13) that in the first case is much lower than in the second one.

The global RVE responses have to be compared with the Eq. (1) stress-strain curves resulting from an equivalent load process. This comparison allows to determine the Tvergaard correction coefficients. In the present work, the analytically derived relation is adopted, that:

$$q_3 = q_1^2$$

In the subsequent refinement of the model calibration the parameter q_3 could be live free.

The two remaining free parameters q_1, q_2 are determined by imposing on the homogenized law the condition that the characteristic values:

$$\sigma_{\max}; \qquad \int_0^{\varepsilon_c} \sigma d\varepsilon$$

are equal to that resulting from the FEM calculation.

The first load case (uniaxial strain) is quite insensitive to the parameter variation, due to the very slow void growth rate present in this condition, so the calibration has been done with reference to the second load case. Finally, the resulting values are:

$$q_1 = 1.25; \; q_2 = 0.98.$$

In Fig. 6, the comparison between the FEM model cell and the homogenized law (1) stress-strain curve is reported for the two load cases.

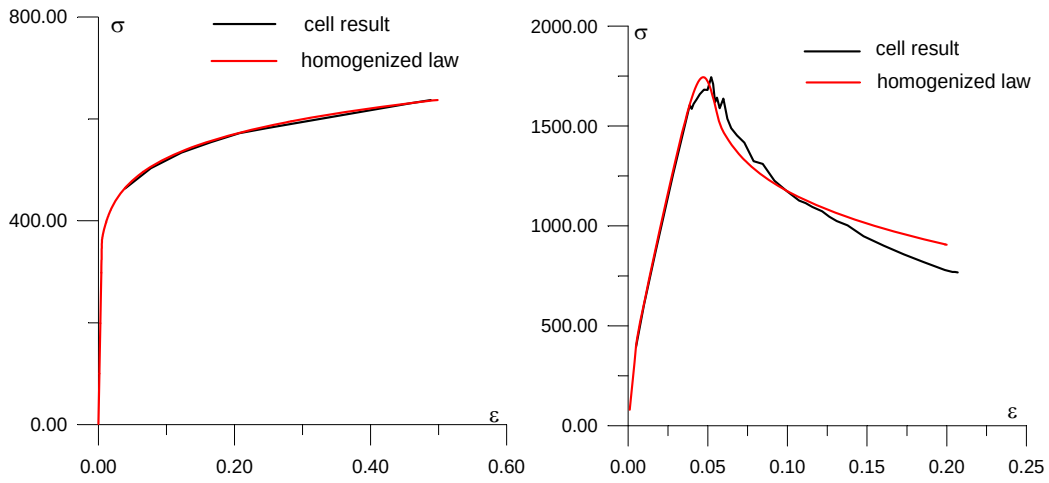

Figure 6: Global cell response compared with Eq. (1) for the two load cases.

In the following Fig. 7 the coalescence law (4) has been included into the constitutive law, with the imposed values f_c = 0.2 for the starting point, and λ = 0.1 for the curve slope, as established before. It is shown that the energy related to the coalescence process is a non negligible part of the total cell energy.

Nucleation parameters

In the present work, the nucleation parameters have been considered as correction parameters, not directly related to the microstructure. Then, the parameters f_N, ε_N , S_N have been used to fit the experimental-numerical results in the residual strength curve, and their values are reported in the following section.

R-CURVE DETERMINATION

The R-curve calculation procedure has been tested on an M(T) specimen model, which experimental results have been published in [13].

The M(T) specimen used for the residual strength results is made by a 1.28 mm thick 2024 sheet material. The panel width is W = 500 mm and the initial half crack length is a_0 = 49.78 mm. Testing and data evaluation were done according to ASTM specification E561-86 for R-curve determination. The residual strength tests were done under displacement control.

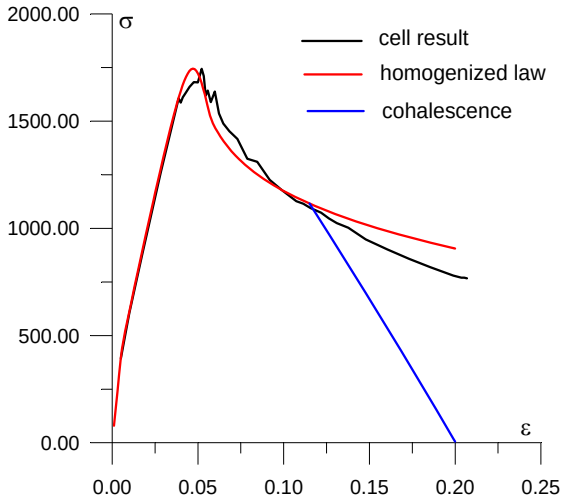

Figure 7: Global cell response compared with eq. (1) and the coalescence law.

Mesh generation

The FEM mesh has been generated within the ANSYS code pre-processor module. All the elements are eight nodes brick, in order to be allowable for the subsequent calculations with the WARP3D [14] solver. The specimen has been modelled taking into account the three symmetry conditions. Along the crack plane, all the elements are cubic with length D = 106.667 μm (see the calibration section). Along the thickness t, six elements have been generated, so that $t/2$ = 0.64 mm = 6D. In Fig. 8 some particulars of the mesh generation are reported.

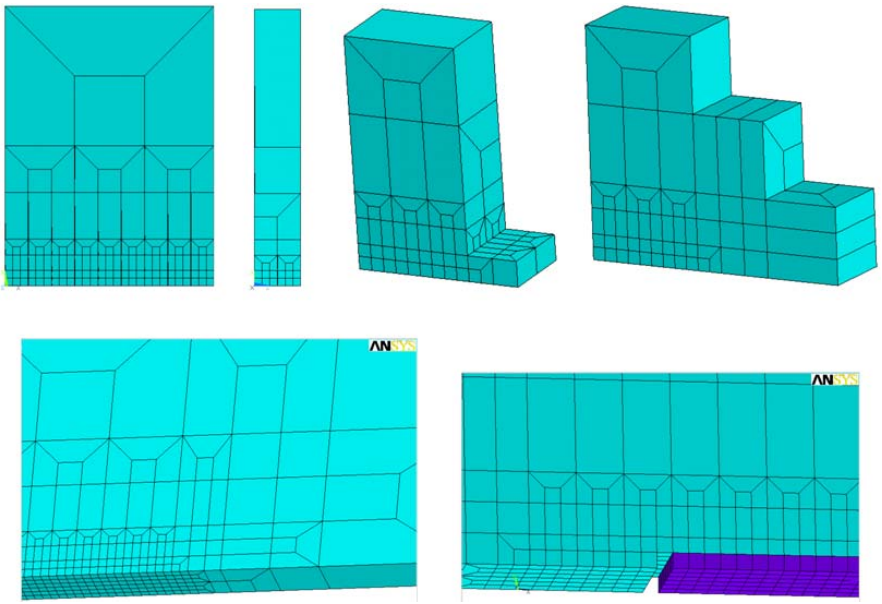

Figure 8: Mesh generation.

It should be noted that, as shown in the last picture, there isn't the row of elements before the initial crack front. Further, the elements that will be killed during the crack advance simulation are indicated with a different colour, that indicates two different materials. In fact, for computational reasons, the killable elements have to be separated from the non-

killable ones; otherwise, the solver can try to kill the above elements in contrast with the crack plane definition. This contrast will produce a fatal error (the limitation is related only to the force-release kill procedure). The elements immediately before the initial crack front have been deleted in order to avoid an undesired 'collaboration' to the initial crack strength.
The as generated mesh, and the boundary conditions can be 'translated' into the corresponding WARP3D commands by using a Fortran routine.

Results: Load vs. crack length curve

From the experimental test data, the following material parameters have been chosen for the numerical analysis:

E = 71100 MPa
σ_y = 366 MPa
σ_u = 482 MPa
ε_f = 0.173

So, the internal stress parameters are (see the calibration chapter):

$\sigma_0 = \sigma_y$ = 366 MPa
$\varepsilon_0 = \sigma_y / E$ = 0.00515
$\varepsilon_{f,log} = log(1 + \varepsilon_f)$ = 0.1596
$\sigma_{u,true} = \sigma_u(1+ \varepsilon_f)$ = 565 MPa
$N = log(\varepsilon_{f,log} / \varepsilon_0) / log(\sigma_{u,true} / \sigma_0)$ = 8.0

The other constitutive law parameters value, calculated in the above chapter, are:

q_1 = 1.25
q_2 = 0.98
$q_3 = q_1^2$ = 1.56
f_0 = 0.0014
D = 0.10667 mm
f_c = 0.2
λ = 0.1

After the solution has been calculated, by using a Fortran routine, the WARP3D output file can be read and interpreted. For every step, the total reaction value R_y in the traction direction and the total number of killed elements Nk are stored. Then, with simple transformations, the gross stress S and the half crack length a are pointed out:

$S = R_y / (t \cdot W/4)$
$a = Nk / (t/2) \cdot D^2$

The resulting curve $S(a)$ has to be compared with the experimental curve in order to perform the tuning of the nucleation parameters.

Nucleation parameters tuning

From the afore cited experimental test data, the following experimental stress vs. crack length curve results (Fig. 9).
By varying the nucleation parameters ε_N , S_N, f_N , different curves have been calculated . The parameter f_N gets down the curve when it is increased; S_N has the opposite effect, with a little influence on the shape of the curve; the increasing of ε_N can slightly move the curve maximum value versus the increasing Δa. The best nucleation parameters are:

ε_N = 0.09
S_N = 0.09
f_N = 0.2

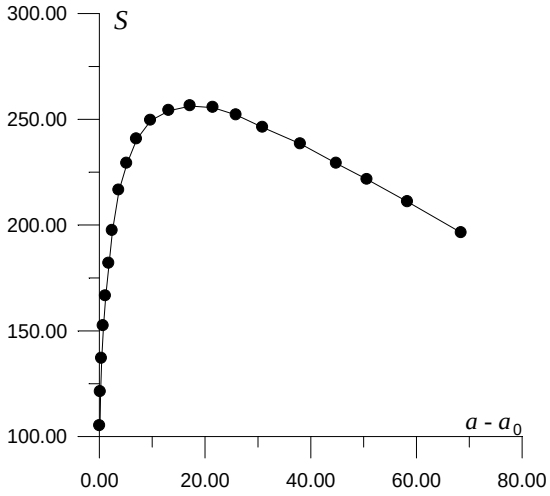

Figure 9: Experimental stress vs. crack length curve.

Final results and R-curve

The ASTM specification E561-86 for R-curve determination imposes that the curves have to be expressed in terms of equivalent stress intensity factor and equivalent crack length, in order to take into account for the plastic deformation around the crack tip.

For the M(T) central crack specimen, the equivalent SIF is:

$$K_{eq} = \sec\left(\frac{\pi a_{eq}}{W}\right) S\sqrt{\pi a_{eq}} = \beta\left(a_{eq}\right) S\sqrt{\pi a_{eq}} \tag{5}$$

The equivalent crack length has two alternative definition: the one, based on the Crack Opening Displacement in the traction direction of the centre of the crack; the other, that has been adopted in the present work, based on the plastic radius evaluation.

The plasticity contribution to the crack length is done by:

$$r_p = \frac{1}{2\pi}\left(\frac{K_{eq}}{\sigma_y}\right)^2 \tag{6_1}$$

The equivalent crack length is defined by:

$$a_{eq} = a + r_p; \quad \Delta a_{eq} = a_{eq} - a_0 \tag{6_2}$$

The plastic radius definition (6) contains the equivalent SIF and, vice-versa, the expression (5) contains the equivalent crack length. It is then necessary to calculate iteratively the two expressions (5), (6) up to the convergence is reached.

The current plastic radius value is done by:

$$r_p^{i+1} = \frac{1}{2\pi}\left(\frac{\beta\left(a + r_p^i\right) S\sqrt{\pi\left(a + r_p^i\right)}}{\sigma_y}\right)^2; \quad r_p^1 = \frac{1}{2\pi}\left(\frac{\beta(a) S\sqrt{\pi a}}{\sigma_y}\right)^2$$

The convergence is reached when the $(i+1)$-th value of the plastic radius differs from the i-th value for a 'small' quantity.

By using the $S(a)$ values calculated before, and after the above descript transformation $(S, a) \rightarrow (K_{eq}, a_{eq})$, we can compare the calculated and experimental R-curves, as reported in Fig. 10.

As a result, the calculated R-curve is in very good agreement with the experimental test.

In the following pictures, some results from the FEM solution are reported. The WARP3D solution data stored during the calculation has been 'translated' in ANSYS commands with a Fortran routine, in order to use its postprocessor module.

In Fig. 11 the calculated stress distribution in the traction direction (y) for the half-crack length increasing Δa = 25 mm is reported for the whole model and near the crack front. It is possible to appreciate the thorough-the-thickness distribution (remember that symmetry conditions have been imposed).
In the following Fig. 12, the crack front shape is pointed out. It results from the elements extinction procedure above descript.

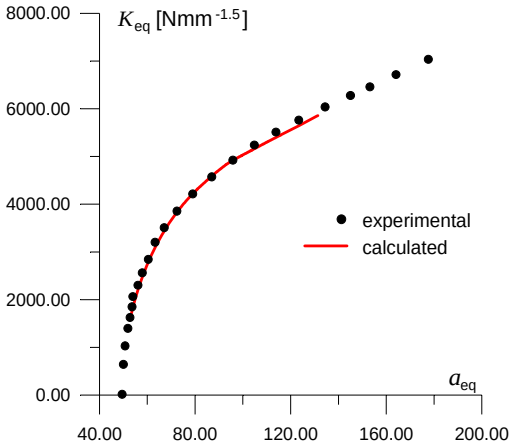

Figure 10: Comparison between calculated and experimental R-curve.

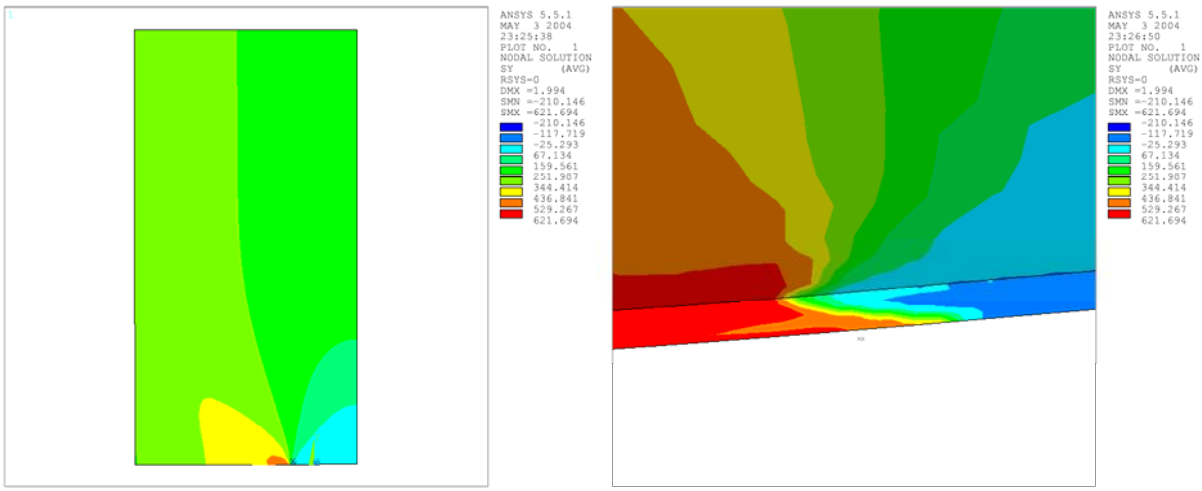

Figure 11: Calculated stress distribution in the traction direction (y) for Δa = 25 mm.

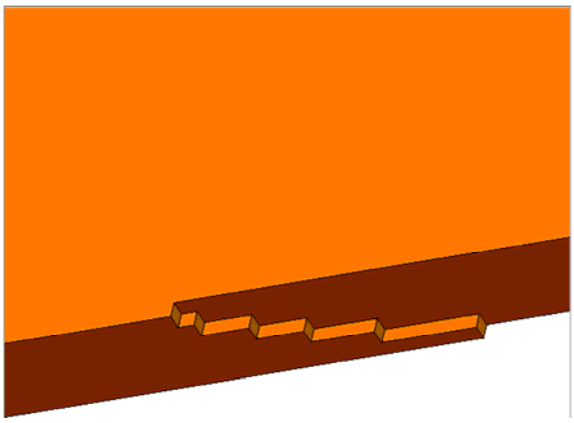

Figure 12: Crack front shape resulting from elements extinction.

In Fig. 13, the enhanced deformed configuration is reported, for Δa = 25 mm. In the first picture, the deformation around the crack tip is pointed out ant it is possible to appreciate the strain localization effect. In the last picture, the residual strain near the initial crack length is shown. Considering that the crack surface is stress free, the deformation is totally plastic. Further, the difference between the residual strain on the symmetry surface (the visible surface) and the external one is shown, were for the external surface (near the plane stress condition) the plastic strain is much higher.

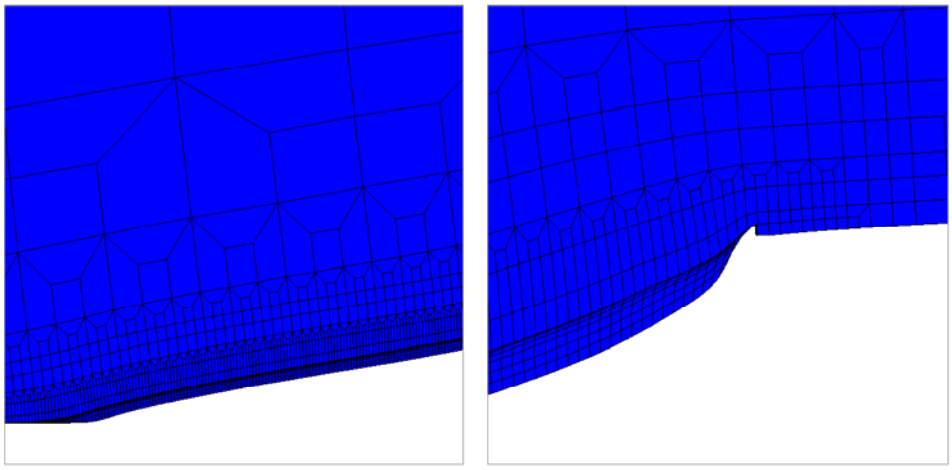

Figure 13: Deformed configuration near the crack tip and the initial crack length.

CONCLUSIONS

A complete procedure for the R-curve calculation has been presented, that gives results in a very good agreement with the experimental tests. The algorithm, based on the Gurson – Tvergaard damage model, uses a preliminary RVE definition, partially based on microstructural information on the material, to determine most of the continuum-scaled model. Only few parameters are tuned on the basis of an experimental test, that are the nucleation parameters f_N, ε_N, S_N. They are related to the material behaviour, nor to the geometry of the test specimen. For this reason, they can reasonably determined with a single test result, as is done in the present work, and the same values can be used for different geometries, as the design process requires.

REFERENCES

[1] Bradley Dodd, Yilong Bai – "Ductile Fracture and Ductility", Academic Press Inc. Ldt., Orlando (Florida), (1987).
[2] Ming Li, Int. J. Mech. Science, 42 (2000) 907.
[3] Lin Xia, C. Fong Shih, John W. Hutchinson, J.Mech. Phys., Solids, 43 (3) (1995) 389.
[4] Lin Xia, C. Fong Shih, J.Mech. Phys., Solids, 43 (2) (1995) 233.
[5] Lin Xia, C. Fong Shih, J.Mech. Phys., Solids, 43 (12) (1995) 1953.
[6] Lin Xia, C. Fong Shih, J.Mech. Phys., Solids, 44 (4) (1996) 603.
[7] C. Ruggieri, T. L. Panontin, R. H. Dodds Jr, Int. J. of Fracture, 82 (1996) 67.
[8] Faleskog J, Gao X, Shih CF., Int. J. of Fracture, 89 (1998) 355.
[9] Gao X, Faleskog J, Shih CF., Int. J. of Fracture 89 (1998) 375.
[10] Z.L. Zhang, C. Thaulow, J. Odegard, Engineering Fracture Mechanics 67 (2000) 155.
[11] M. Hori, S. Nemat-Nasser, Mech. of Materials 31 (1999) 667.
[12] J. F. Ganghoffer, L.J. Sluys, R. De Borst, Eur. J. Mech. Solids, 18 (1) (1999), 17.
[13] Office of Aviation Research - 'Residual Strength Test on Stiffened Panels With Multiple-Site Damage', technical report, Washington, D.C. 20591 [www.tc.faa.gov/its/act141/reportpage.html].
[14] Arne S. Gullerud, Kyle C. Koppenhoefer, Arun Roy, Robert H. Dodds, Jr. - WARP3D–Release 13.9 - Department Of Civil Engineering University of Illinois at Urbana–Champaign Urbana, Illinois, September 2000 - ISSN: 0069–4274.